An asymmetric-friction based model for magnetorheological dampers ⋆

I. García-Baños * **F. Ikhouane** * **N. Aguirre-Carvajal** **

* *Universitat Politècnica de Catalunya, Department of Mathematics. Barcelona East School of Engineering, carrer Eduard Maristany, 16, 08019, Barcelona, Spain.*
isabel.garcia.banos@estudiant.upc.edu, faycal.ikhouane@upc.edu
** *naguirreca@unal.edu.co*

Abstract
The modeling of magnetorheological dampers combines the use of the laws of physics along with a phenomenological description. The phenomenological models that are used to describe these devices present a symmetric hysteresis loop. However, the experimental hysteresis loops of MR dampers are not symmetric. To take into account this asymmetry, we propose a modification of the viscous + Dahl model, use the modified model to describe a large-scale magnetorheological damper, and validate the modified model against experimental data.

Keywords: Magnetotheological dampers, modeling, identification.

1. INTRODUCTION

Magnetorheological (MR) fluids consist of a non-magnetic fluid carrier that contains magnetic particules. When a magnetic field is applied, the magnetic particles form chains that impede the flow of the fluid carrier. The MR fluid becomes then semisolid with a viscoplastic behavior that depends on the magnitude of the magnetic field.

MR dampers are devices that use MR fluids to generate a friction force that can be adjusted by using different levels of the magnetic field. These devices can be seen as systems with two inputs and one output. The inputs are (1) the current or voltage v that generates the magnetic field, and (2) the displacement x or rotation angle of the device. The output is the friction force F that opposes the movement of the damper, see Figure 1.

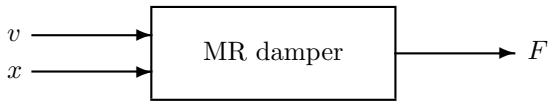

Figure 1. Input-output description of a MR damper

MR dampers have applications in several fields that include vehicle systems, Choi et al. (2013); Savaresi et al. (2005), biomedical engineering, Xi et al. (2016), and civil engineering, Raju et al. (2013).

Owing to the complex nonlinear behavior of MR dampers, their modeling usually combines physical considerations along with a phenomenological description. A review of the models used for MR dampers may be found in Imaduddin et al. (2013). The authors list the following models for having been used to represent the behavior of MR dampers: the Bingham model, the Herschel–Bulkley model, the Bouc-Wen model, and the Dahl model. The Preisach model is considered in Section 3.2 of Choi et al. (2013) and the LuGre model is used by Yu et al. (2015).

All these models share a common property: their hysteresis loop -of the dry friction force in steady-state versus displacement- is symmetric with respect to its center. Indeed, the analytical expression of the hysteresis loop of the Bouc-Wen model and that of its particular case the Dahl model, are calculated by Ikhouane et al. (2005), whilst the analytical expression of the hysteresis loop of the LuGre model is provided by Naser et al. (2015).

However, as shown in Section 5 of the present paper, the experimentally obtained hysteresis loop of the MR damper is not symmetric. Thus there is a need to modify the models that represent MR dampers in order to accomodate this asymmetry.

In this paper we use the viscous + Dahl model to represent a large-scale MR damper. Our choice of this model stems from the following considerations:

(1) Like the Coulomb model, the Bingham and the Herschel–Bulkley models are static, thus leading to inconsistencies when the velocity changes, see García-Baños et al. (2016).
(2) The Bouc-Wen model is dynamic. However, it is shown by Ikhouane et al. (2007) that, when applied to the modeling of MR dampers, the Bouc-Wen model can be approximated by the Dahl model.
(3) The Preisach model is much more complex than the Dahl model which hinders its use for control purposes.

Since the Dahl model generates a symmetric hysteresis loop, we modify the original model in order to obtain an asymmetric hysteresis loop. This modification is done in

⋆ Supported by the Spanish Ministry of Economy, Industry and Competitiveness through grant DPI2016-77407-P (AEI/FEDER, UE).

such a way to preserve other properties of the original Dahl model that are consistent with experimental observations.

The paper is structured as follows. Section 2 provides the characteristics of the MR damper used for the experiments. Section 3 presents the viscous + Dahl model used by Aguirre-Carvajal et al. (2012) to model the MR damper. Section 4 proposes a methodology for the identification of the unknown model parameters. This methodology is used in Section 5 to show that the hysteresis loop of the MR damper is not symmetric. To accomodate this asymmetry, a modification of the viscous + Dahl model is proposed in Section 6. The parameters of this modified model are identified using the methodology presented in Section 4, and the model is validated against experimental data in Section 7. Conclusions are presented in Section 8.

2. THE LARGE-SCALE MR DAMPER

The large-scale MR damper used in the experiments has been manufactured by Lord Corporation. It is located at the University of Colorado at Boulder Network for Earthquake Engineering Simulation Fast Hybrid Test facility (see Figure 2). The damper has an available stroke of 584 mm and can provide forces that range from 15 to 200 kN. The displacements are measured with MTS 244.51S/244.41S displacement transducers. The damper force is measured with MTS 661.31E-01/661.23E-01 force transducers. The other technical details relative to this MR damper are provided in Section 2 of the paper by Aguirre-Carvajal et al. (2012).

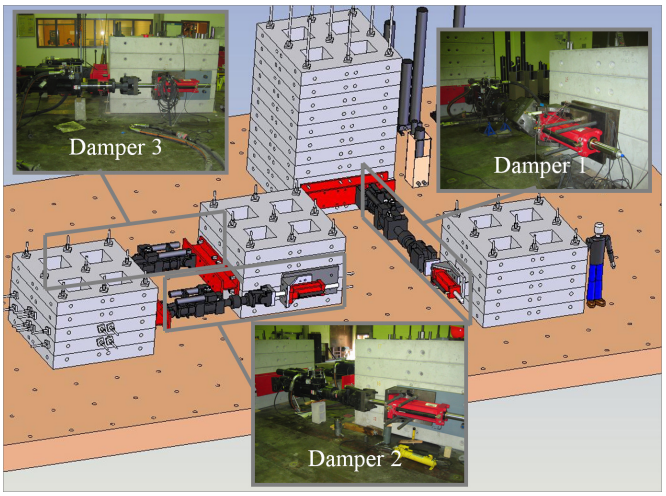

Figure 2. MR damper 1 is used for the experiments

Recall that the damper produces only a friction force that opposes the movement of the piston. Thus, to complete the experimental setting, a hydraulic actuator is coupled to the damper in order to impose a given displacement of the piston.

The equation of the movement of the piston is given by Newton's second law

$$m\ddot{x}(t) = F_h(t) - F(t), \tag{1}$$

where m is the mass of the piston, x its displacement, $\ddot{x}$ its acceleration, t is time, $\boldsymbol{F}_h = F_h\boldsymbol{i}$ is the force applied by the hydraulic actuator, $\boldsymbol{F} = -F\boldsymbol{i}$ the friction force generated by the damper, and $\boldsymbol{i}$ is the unit vector along the x–axis, see Figure 3.

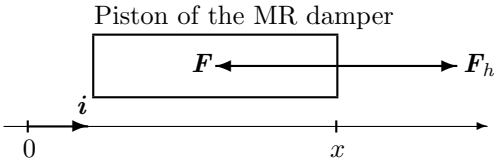

Figure 3. Piston of the MR damper

3. THE VISCOUS + DAHL MODEL

The aim of this section is to introduce the viscous + Dahl model used by Aguirre-Carvajal et al. (2012) to describe the MR damper of Section 2.

The friction force F is considered to be decomposed as the sum of a dry friction force F_d and a viscous friction force F_v, that is

$$F = F_d + F_v. \tag{2}$$

The Coulomb model expresses the dry friction force as a function of a constant relative velocity of the piston as (Coulomb, 1821, pp. 41–42)

$$F_d = \kappa_w \text{ for } \dot{x} > 0, \tag{3}$$

where $\kappa_w > 0$ is the Coulomb friction level.

It is customary in the current literature to add to Equation (3) the following two equations

$$F_d = -\kappa_w \text{ for } \dot{x} < 0, \tag{4}$$

$$-\kappa_w \leq F_d \leq \kappa_w \text{ for } \dot{x} = 0, \tag{5}$$

to complete the description of the dry friction force, although Coulomb (1821) did not report Equations (4)–(5).

Equation (3) is consistent with experimental observations for constant velocities $\dot{x}$. However, when the velocity changes, this may no longer be the case, see García-Baños et al. (2016). For this reason, Dahl (1976) proposed a model that relates the dry friction force F_d to the relative velocity as

$$F_d(t) = \kappa_w w(t), \tag{6}$$

$$\dot{w}(t) = \rho\big(\dot{x}(t) - |\dot{x}(t)|w(t)\big), \tag{7}$$

$$-1 \leq w(0) \leq 1, \tag{8}$$

where w is an internal state variable, and $\rho > 0$ is a constant.

The relationship between the Dahl model and the Coulomb model is studied in detail by García-Baños et al. (2016) who show that the Dahl model is compatible with the Coulomb model for constant velocities, and that the dry friction given by the Dahl model is a continuous function of time for varying velocities (this is not the case for the Coulomb model).

The viscous friction force is assumed to be given by

$$F_v(t) = \kappa_x \dot{x}(t) \tag{9}$$

where $\kappa_x > 0$ is a constant.

The viscous + Dahl model relates the friction force F to the displacement x as

$$F(t) = \kappa_x \dot{x}(t) + \kappa_w w(t), \tag{10}$$

$$\dot{w}(t) = \rho\big(\dot{x}(t) - |\dot{x}(t)|w(t)\big), \tag{11}$$

$$-1 \leq w(0) \leq 1. \tag{12}$$

The model (10)–(12) has been used by Aguirre-Carvajal et al. (2012) to describe the MR damper of Section 2. The

coefficients κ_x and κ_w have been shown to depend on the voltage input.

In the present paper we consider the voltage to be constant in order to simplify the presentation of the modified model. When the voltage varies, the coefficients κ_x and κ_w can be modeled as in Aguirre-Carvajal et al. (2012).

With this in mind, the MR damper can be seen as a system whose input is the displacement x and whose output is the force F, see Figure 4.

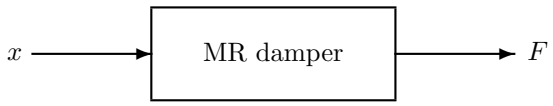

Figure 4. MR damper

4. PARAMETER IDENTIFICATION

In Equations (10)–(11) the parameters κ_x, κ_w and ρ are usually unknown, so that they have to be identified from input-output data. To this end, the following result is useful.

Proposition 1. Let $b > 0$ be a strictly positive real number. If $\dot{x}(t) \geq b, \forall t \geq 0$ then $\lim_{t\to\infty} w(t) = 1$, and if $\dot{x}(t) \leq -b, \forall t \geq 0$ then $\lim_{t\to\infty} w(t) = -1$.

Proof. Assume that $\dot{x}(t) \geq b > 0, \forall t \geq 0$. Using the Comparison Lemma (Khalil, 2000, p. 102) it comes from Equation (7) and (García-Baños et al., 2016, Equation (18)) that

$$w(t) \geq 1 - \big(1 - w(0)\big)e^{-\rho b t}, \forall t \geq 0. \tag{13}$$

On the other hand, it follows from Inequalities (8) and (Ikhouane et al., 2005, Table 2) that $w(t) \leq 1, \forall t \geq 0$. This fact combined with Inequality (13) shows that $\lim_{t\to\infty} w(t) = 1$ which ends the proof.

Suppose that we impose a velocity $\dot{x}$ larger than $b > 0$, then from (10) we get in steady-state by Proposition 1 that

$$F = \kappa_x \dot{x} + \kappa_w. \tag{14}$$

Since F and $\dot{x}$ are available from experiments, a linear regression on (14) provides κ_x and κ_w.

To avoid computing $\dot{x}$, Equation (14) can also be written as

$$\frac{\int_{t_0}^{t} F(\tau)\,\mathrm{d}\tau}{t - t_0} = \kappa_x \frac{x(t) - x(t_0)}{t - t_0} + \kappa_w, \quad t > t_0, \tag{15}$$

which provides κ_x and κ_w using a linear regression.

To identify the parameter ρ we use a displacement signal x that is wave periodic: this means that there exist constants $0 < T^+ < T$ such that x satisfies Properties (i)-(iv).

(i) x is continuous on $\mathbb{R}_+$.
(ii) x is T-periodic.
(iii) x is continuously differentiable on $(0, T^+)$ and on (T^+, T).
(iv) x is strictly increasing on $(0, T^+)$ and is strictly decreasing on (T^+, T).

An example of such a signal is provided in Figure 6. Consider that a wave-periodic displacement is imposed by the hydraulic actuator. Then, the state w that appears in Equation (11) has a transient and a steady-state $\bar{w}$. This steady-state has an increasing part $\bar{w}_\uparrow$ that corresponds to an increasing displacement, and a decreasing part $\bar{w}_\downarrow$ that corresponds to a decreasing displacement (see Ikhouane et al. (2005) for a proof).

The equations for $\bar{w}_\uparrow$ and $\bar{w}_\downarrow$ are detailed in García-Baños et al. (2016) as

$$a = \frac{2}{1 + e^{-\rho(X_{\max} - X_{\min})}}, \tag{16}$$

$$\bar{w}_\uparrow(x) = 1 - ae^{-\rho(x - X_{\min})}, \quad \forall x \in [X_{\min}, X_{\max}], \tag{17}$$

$$\bar{w}_\downarrow(x) = -1 + ae^{\rho(x - X_{\max})}, \quad \forall x \in [X_{\min}, X_{\max}], \tag{18}$$

where $X_{\min} < X_{\max}$ correspond to the smallest and largest values of the displacement x. Equations (16)–(18) describe the hysteresis loop $\bar{w}$ versus x, see Figure 5.

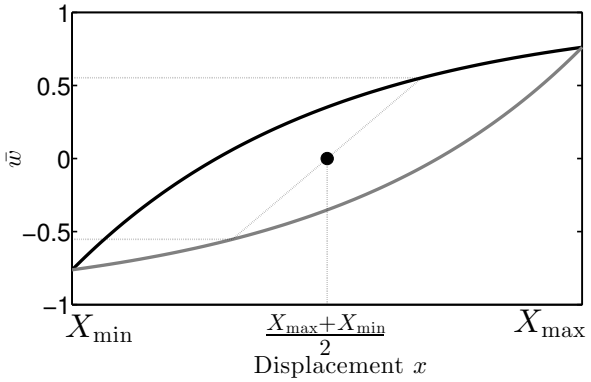

Figure 5. Black: $\bar{w}_\uparrow$ versus x. Grey: $\bar{w}_\downarrow$ versus x. The point $\big(\frac{X_{\max}+X_{\min}}{2}, 0\big)$ is a center of symmetry for the hysteresis loop $\bar{w}$ versus x.

The area enclosed within the hysteresis loop can be calculated as follows

$$\int_{X_{\min}}^{X_{\max}} \bar{w}_\uparrow(x) - \bar{w}_\downarrow(x)dx = 2(X_{\max} - X_{\min})\big(1 - f(\nu)\big) \tag{19}$$

where $\nu = \rho(X_{\max} - X_{\min})$, $f : \mathbb{R}_+ \to \mathbb{R}_+$ is defined by $f(z) = \frac{2}{z}\tanh\left(\frac{z}{2}\right), \forall z > 0$, $f(0) = 1$, and tanh sets for the hyperbolic tangent. It can be checked that f is right-continuous at 0. We also have

$$f'(z) = \frac{2}{z^2}\left[\frac{z}{2}\left(1 - \tanh^2\left(\frac{z}{2}\right)\right) - \tanh\left(\frac{z}{2}\right)\right], \forall z > 0.$$

Define the function $g : \mathbb{R}_+ \to \mathbb{R}$ by

$$g(z) = \frac{z}{2}\left(1 - \tanh^2\left(\frac{z}{2}\right)\right) - \tanh\left(\frac{z}{2}\right), \forall z \geq 0.$$

Then, $\forall z > 0$ we have

$$g'(z) = -\frac{z}{2}\tanh\left(\frac{z}{2}\right)\left(1 - \tanh^2\left(\frac{z}{2}\right)\right). \tag{20}$$

Since $z > 0$ we have $\tanh\left(\frac{z}{2}\right) > 0$. Also $1 - \tanh^2\left(\frac{z}{2}\right) > 0$ as the absolute value of the hyperbolic tangent is always strictly less than 1. Thus $g'(z) < 0, \forall z > 0$ so that g is strictly decreasing. In particular we have $g(z) < g(0) = 0, \forall z > 0$. Thus $f'(z) < 0, \forall z > 0$ which means that f is strictly decreasing.

Define the function $h : \mathbb{R}_+ \to \mathbb{R}_+$ by

$$h(\nu) = 1 - \frac{2}{\nu}\tanh\left(\frac{\nu}{2}\right), \forall \nu > 0$$

and

$$h(0) = 0.$$

Then, h is right-continuous at 0, and is strictly increasing so that it is invertible.

With this in mind, ρ is identified as follows. If we know the area of the hysteresis loop from experimental data, that is if we know the quantity $\int_{X_{\min}}^{X_{\max}} \bar{w}_{\uparrow}(x) - \bar{w}_{\downarrow}(x)dx$ we can compute $h(\nu)$ since by Equation (19)

$$\frac{\int_{X_{\min}}^{X_{\max}} \bar{w}_{\uparrow}(x) - \bar{w}_{\downarrow}(x)dx}{2(X_{\max} - X_{\min})} = h(\nu).$$

Once $h(\nu)$ has been computed we can find ν as h is invertible. Then ρ is calculated as

$$\rho = \frac{\nu}{X_{\max} - X_{\min}}.$$

5. EXPERIMENTAL OBSERVATIONS

We fix the voltage input to 0.5 V. Using the hydraulic actuator, we impose the wave-periodic displacement of Figure 6. The corresponding output force is provided in

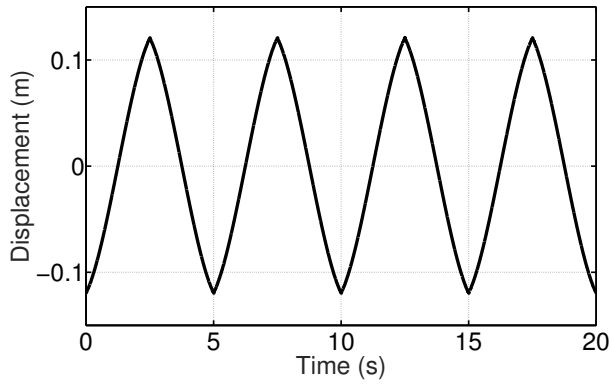

Figure 6. Displacement of the damper versus time

Figure 7. We observe that the force reaches rapidly a steady-state periodic response. We use the fourth period of the force response to calculate the unkown parameters κ_x, κ_w and ρ. This period corresponds to the time interval $[15, 20]$ s.

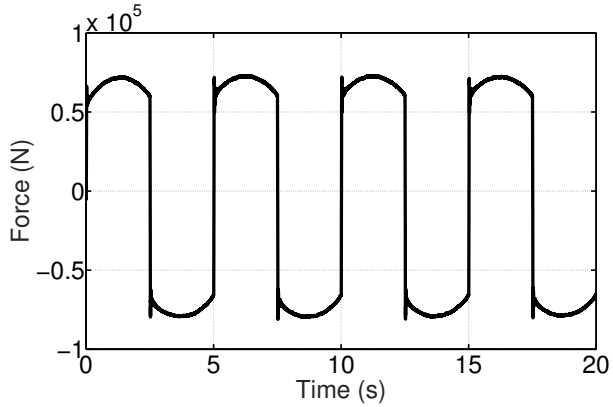

Figure 7. Force versus time

Since the displacement x is available from direct measurements, we can calculate $\dot{x}$ using an Euler approximation. Figure 8 provides the velocity $\dot{x}$ that corresponds to an increasing displacement in the fourth period.

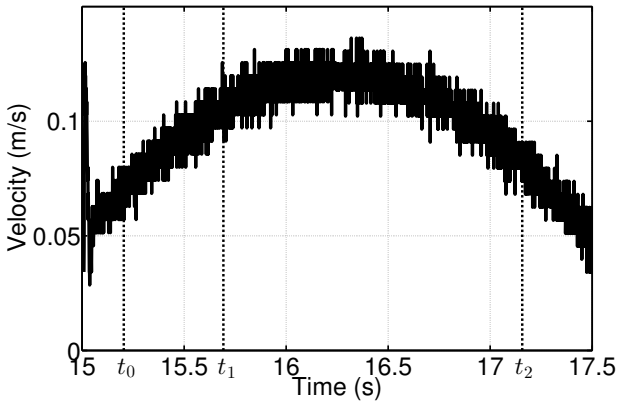

Figure 8. Velocity versus time

Observe that at the points $t = 15$ s and $t = 17.5$ s the velocity is not defined since the displacement is not differentiable at these points. We can see from Figure 8 that $\dot{x}(t) > 0.01$ m/s for all $t \in (15, 17.5)$ s so that, by Proposition 1, Equation (15) holds for all $t \in [t_0, 17.5)$ where $15 < t_0 < 17.5$.

We take $t_0 = 15.2041$ s, $t_1 = 15.6924$ s and $t_2 = 17.1572$ s, see Figure 8. A linear regression on (15) using the time interval $t \in [t_1, t_2]$ provides $k_{x1} = 1.6299 \cdot 10^5$ kg/s and $k_{w1} = 5.2620 \cdot 10^4$ N where the index 1 is used to indicate that these values correspond to an increasing displacement.

Figure 9 provides two plots: the regression line $\beta = k_{x1}\alpha + k_{w1}$ where $\alpha \in [0.0804, 0.1067]$ m/s, and the set of experimental points $\left(\frac{x(t)-x(t_0)}{t-t_0}, \frac{\int_{t_0}^{t} F(\tau)\,\mathrm{d}\tau}{t-t_0} \right)$ where $t \in [t_1, t_2]$, $F(\tau)$ is the measured force at instant $\tau \in [t_1, t]$ and $x(t)$ the measured displacement at instant t.

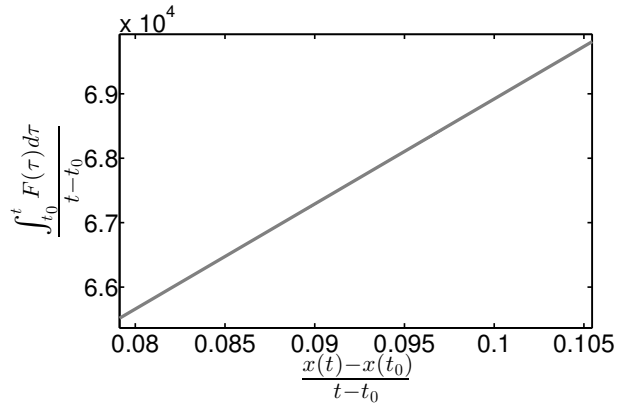

Figure 9. Grey: Regression line $\beta = k_{x1}\alpha + k_{w1}$. Black: Experimental points $\left(\frac{x(t)-x(t_0)}{t-t_0}, \frac{\int_{t_0}^{t} F(\tau)\,\mathrm{d}\tau}{t-t_0} \right)$ where $t \in [t_1, t_2]$.

We observe that the points $\left(\frac{x(t)-x(t_0)}{t-t_0}, \frac{\int_{t_0}^{t} F(\tau)\,\mathrm{d}\tau}{t-t_0}\right)$ lie almost exactly on the regression line $\beta = k_{x1}\alpha + k_{w1}$. This experimental fact provides a justification *a posteriori* that, in Proposition 1, if we consider the initial time as the instant 15 s, then the time interval $[t_0, 17.5)$ corresponds to a steady-state in which w is equal to 1.

Similarly, when the displacement is a decreasing function of time, that is in the time interval $[17.5, 20]$ s, we compute the parameters $k_{x2} = 1.3352 \cdot 10^5$ kg/s and $k_{w2} = 6.2986 \cdot 10^4$ N. We also observe that the experimental points $\left(\frac{x(t)-x(t_0)}{t-t_0}, \frac{\int_{t_0}^{t} F(\tau)\,\mathrm{d}\tau}{t-t_0}\right)$ lie almost exactly on the regression line $\beta = k_{x2}\alpha + k_{w2}$, see Figure 10.

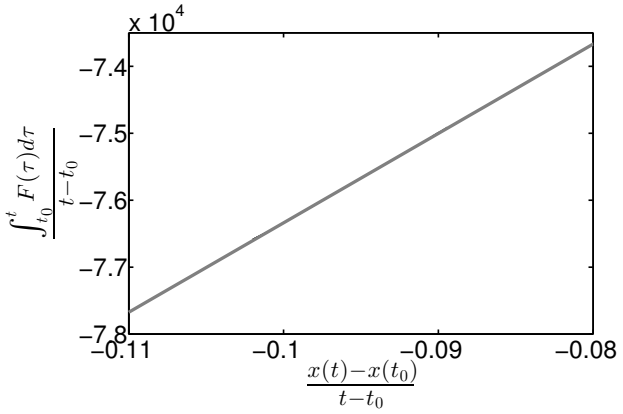

Figure 10. Grey: Regression line $\beta = k_{x2}\alpha + k_{w2}$. Black: Experimental points $\left(\frac{x(t)-x(t_0)}{t-t_0}, \frac{\int_{t_0}^{t} F(\tau)\,\mathrm{d}\tau}{t-t_0}\right)$ where $t \in [t_1, t_2]$.

Note that $k_{x1} = 1.6299 \cdot 10^5 \neq 1.3352 \cdot 10^5 = k_{x2}$ and $k_{w1} = 5.2620 \cdot 10^4 \neq 6.2986 \cdot 10^4 = k_{w2}$. This observation shows that the model (10)–(12) does not represent accurately the real behavior of the MR damper since the model considers that $k_{x1} = k_{x2} = \kappa_x$ and $k_{w1} = k_{w2} = \kappa_w$.

6. THE MODIFIED MODEL

The aim of this section is to propose a modification of the model (10)–(12) that incorporates coefficients κ_x and κ_w that change when the velocity changes sign. One may think to change (10)–(12) into

$$F(t) = \kappa_{x1}\dot{x}(t) + \kappa_{w1}w(t), \text{ when } \dot{x}(t) > 0, \tag{21}$$
$$F(t) = \kappa_{x2}\dot{x}(t) + \kappa_{w2}w(t), \text{ when } \dot{x}(t) \leq 0, \tag{22}$$
$$\dot{w}(t) = \rho\big(\dot{x}(t) - |\dot{x}(t)|w(t)\big), \tag{23}$$
$$-1 \leq w(0) \leq 1. \tag{24}$$

The model (21)–(24) assumes that the dry friction force F_d is given by

$$F_d(t) = \kappa_{w1}w(t), \text{ when } \dot{x}(t) > 0, \tag{25}$$
$$F_d(t) = \kappa_{w2}w(t), \text{ when } \dot{x}(t) \leq 0. \tag{26}$$

Consider the time instant 17.5 s at which the velocity changes sign. Then

$$\lim_{t\uparrow 17.5} F_d(t) = \kappa_{w1} \lim_{t\uparrow 17.5} w(t)$$

and

$$\lim_{t\downarrow 17.5} F_d(t) = \kappa_{w2} \lim_{t\downarrow 17.5} w(t).$$

The function w is continuous as a solution of the differential equation (23) so that

$$\lim_{t\uparrow 17.5} w(t) = \lim_{t\downarrow 17.5} w(t) = w(17.5).$$

Since the instant 17.5 s corresponds to a steady-state of w, it is given by Equation (17) as $w(17.5) \simeq \bar{w}_{\uparrow}(X_{\max}) \simeq 1$ so that

$$\lim_{t\uparrow 17.5} F_d(t) = \kappa_{w1}w(17.5) \neq \kappa_{w2}w(17.5) = \lim_{t\downarrow 17.5} F_d(t),$$

meaning that the dry friction force F_d is discontinuous at the instant 17.5 s.

However, experimental evidence shows that the dry friction force is a continuous function of time (Armstrong-Helouvry, 1991, p. 40). This means that the model (21)–(24) is not adequate for the description of the MR damper.

As an alternative to the model (21)–(24) we propose the following model:

$$F(t) = F_v(t) + F_d(t), \tag{27}$$
$$\dot{w}(t) = \rho\big(\dot{x}(t) - |\dot{x}(t)|w(t)\big), \tag{28}$$
$$-1 \leq w(0) \leq 1, \tag{29}$$

where the dry friction force F_d is given by

$$F_d(t) = \kappa_{w1}w(t), \text{ when } w(t) \geq 0, \tag{30}$$
$$F_d(t) = \kappa_{w2}w(t), \text{ when } w(t) \leq 0, \tag{31}$$

and the viscous friction force F_v is given by

$$F_v(t) = \kappa_{x1}\dot{x}(t), \text{ when } \dot{x}(t) \geq 0, \tag{32}$$
$$F_v(t) = \kappa_{x2}\dot{x}(t), \text{ when } \dot{x}(t) \leq 0. \tag{33}$$

It can be checked that, for the model (27)–(33), the dry friction force is a continuous function of time. This model is also consistent with Coulomb Equation (3) since for a constant velocity $\dot{x} > 0$ we get $\lim_{t\to\infty} F_d(t) = \kappa_{w1}$ by Proposition 1.

The main departure of our model from Equations (3)–(5) and (10)–(12) is that the model (27)–(33) allows the friction constants κ_{x2} and κ_{w2} to be different from their counterparts κ_{x1} and κ_{w1}. This fact results in an asymmetric hysteresis loop F_d in steady-state versus x.

7. MODEL VALIDATION

The aim of this section is to validate the model (27)–(33) against experimental data. To this end we proceed as follows.

Note that κ_{x1} and κ_{x2} have been determined in Section 5. Moreover, the input displacement x has been designed in such a way that $|\dot{x}(t)| > 0.01$ m/s at all instants t where the velocity is defined. This fact makes it possible to decide whether $\dot{x}(t)$ is positive or negative even in the presence of noise (see Figure 8). Thus, the viscous friction force F_v can be effectively calculated from Equations (32)–(33).

Now that F_v is available, the dry friction force F_d can be calculated from Equation (27) as $F_d = F - F_v$.

Observe that Equations (30)–(31) are equivalent to

$$w(t) = \frac{F_d(t)}{\kappa_{w1}}, \text{ when } F_d(t) \geq 0, \tag{34}$$

$$w(t) = \frac{F_d(t)}{\kappa_{w2}}, \text{ when } F_d(t) \leq 0, \tag{35}$$

since $\kappa_{w1} > 0$ and $\kappa_{w2} > 0$. Given that κ_{w1} and κ_{w2} have been determined in Section 5, Equations (34)–(35) provide $w(t)$ for $t \in [15, 20]$ s. Thus the hysteresis loop $\bar{w}$ versus x can be obtained as the set $\big\{\big(x(t), w(t)\big), t \in [15, 20]\big\}$ since we are considering the steady-state response (fourth period).

Now that the experimental hysteresis loop has been determined, the parameter ρ can be computed as in Section 4. We find $\rho = 768.73$ m^{-1}.

The experimental hysteresis loop $\big\{\big(x(t), w(t)\big), t \in [15, 20]\big\}$ is provided in Figure 11 along with the theoretical one obtained from Equations (16)–(18) with the values $\rho = 768.73$ m^{-1}, $X_{\min} = -0.1197$ m and $X_{\max} = 0.1209$ m.

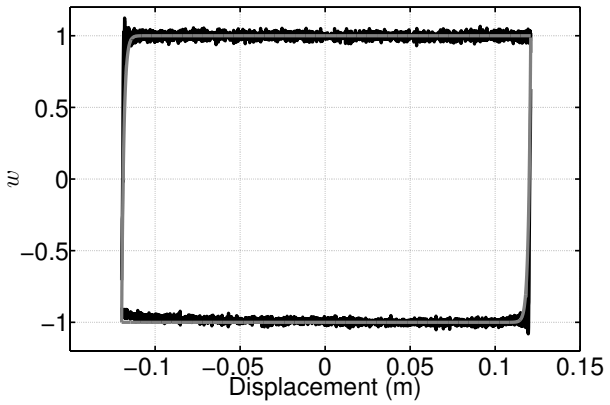

Figure 11. Black: Experimental w obtained from Equations (34)–(35) versus displacement x.
Grey: $\bar{w}_{\uparrow}(x)$ versus x (Equation (17)) and $\bar{w}_{\downarrow}(x)$ versus x (Equation (18)).

We observe that the theoretical hysteresis loop obtained from Equations (16)–(18) is a very good approximation of the experimental hysteresis loop obtained from Equations (34)–(35).

8. CONCLUSIONS

The motivation of the present work is the observation that, for a real MR damper, the friction coefficients κ_{x1} and κ_{w1} that correspond to an increasing displacement are not equal to their counterparts κ_{x2} and κ_{w2} that correspond to a decreasing displacement.

Indeed, the experiments carried out on the MR damper of Section 2 show that κ_{x2} is 18.1% smaller than κ_{x1}, and that κ_{w2} is 19.7% larger than κ_{w1}. The magnitude of these differences justify the use of an alternative model that would incorporate the variation of the friction coefficients with the sense of variation of the displacement.

We have shown that a modification of the viscous + Dahl model that entails different friction coefficients for different signs of the velocity, is not compatible with other properties of the dry friction. For this reason we proposed a model that includes two different sets of friction coefficients, and which, at the same time, is compatible with other properties observed for the dry friction.

We have shown that the proposed model provides a theoretical hysteresis loop that is very close to the one provided by experiments.

REFERENCES

N. Aguirre-Carvajal, F. Ikhouane, J. Rodellar and R. Christenson. Parametric identification of the Dahl model for large scale MR dampers. *Structural Control & Health Monitoring*, volume 19, pages 332–347, 2012.

B. Armstrong-Helouvry. *Control of Machines with Friction*. Kluwer Academic Publishers, 1991.

C.A. Coulomb. *Théorie des Machines Simples, en Ayant Égard au Frottement de Leurs Parties et à la Roideur des Cordages*. [in Gallica, Bibliothèque Nationale de France] Paris, France, 1821.

S.B. Choi and Y.M. Han. *Magnetorheological Fluid Technology. Applications in vehicle systems*. CRC Press, Boca Raton, FL, USA, 2013.

P. Dahl. Solid friction damping of mechanical vibration. *The American Institute of Aeronautics and Astronautics Journal*, volume 14, pages 1675–1682, 1976.

I. García-Baños and F. Ikhouane. A new method for the identification of the parameters of the Dahl model. *Journal of Physics: Conference Series*, volume 744, 012195, 2016.

F. Imaduddin, S.A. Mazlan, H. Zamzuri. A design and modelling review of rotary magnetorheological damper. *Materials and Design*, volume 51, pages 575–591, 2013.

F. Ikhouane and S.J. Dyke. Modeling and identification of a shear mode magnetorheological damper. *Smart Materials and Structures*, volume 16, pages 605-616, 2007.

F. Ikhouane and J. Rodellar. On the hysteretic Bouc-Wen model. Part I: forced limit cycle characterization *Nonlinear Dynamics*, volume 42, pages 63–78, 2005.

H.K. Khalil. *Nonlinear Systems*, Third edition, Upper Saddle River, NJ: Prentice Hall, 2000.

M.F.M. Naser and F. Ikhouane. Hysteresis loop of the LuGre model. *Automatica*, volume 59, pages 48–53, 2015.

K.R. Raju, A.M. Prasad, K. Muthumani, N. Gopalakrishnan, N.R. Iyer, N. Lakshmanan. Experimental studies on use of toggle brace mechanism fitted with magnetorheological dampers for seismic performance enhancement of three-storey steel moment-resisting frame model. *Structural Control & Health Monitoring*, volume 20, pages 373–386, 2013.

S.M. Savaresi, S. Bittanti, M. Montiglio. Identification of semi-physical and black-box non-linear models: the case of MR-dampers for vehicles control. *Automatica*, volume 41, pages 113–127, 2005.

H.L. Xie, Z.B. Liu, J.Y. Yang, Z.Q. Sheng, Z.W. Xu. Modelling of magnetorheological damper for intelligent bionic leg and simulation of knee joint movement control. *International Journal of Simulation Modelling*, volume 15, pages 144–156, 2016.

Y. Yu, Li, Y.C. Li, J.C. Li. Parameter identification and sensitivity analysis of an improved LuGre friction model for magnetorheological elastomer base isolator. *Meccanica*, volume 50(11), pages 2691–2707, 2015.